Stability of waves on fluid of infinite depth with constant vorticity

M. G. Blyth† and E. I. Părău

School of Mathematics, University of East Anglia, Norwich NR4 7TJ, UK

(Received xx; revised xx; accepted xx)

The stability of periodic travelling waves on fluid of infinite depth is examined in the presence of a constant background shear field. The effects of gravity and surface tension are ignored. The base waves are described by an exact solution that was discovered recently by Hur & Wheeler (2020). Linear growth rates are calculated using both an asymptotic approach valid for small amplitude waves and a numerical approach based on a collocation method. Both superharmonic and subharmonic perturbations are considered. Instability is shown to occur for any non-zero amplitude wave.

1. Introduction

The study of water waves has been the focus of intensive research over many years. Most of the work has been devoted to gravity waves on water of finite or infinite depth, but the effects of capillarity have also received significant attention. The issue of wave stability is considered to be particularly important. The experiments on gravity waves that were carried out by Benjamin and Feir in the 1960s provided a particular stimulus. Early analysis (e.g. Lighthill 1965; Benjamin 1967; Benjamin & Feir 1967; Whitham 1967) showed that gravity waves are susceptible to relatively large wavelength subharmonic disturbances that grow in amplitude as the flow develops in what is now usually referred to as Benjamin-Feir instability. Here 'subharmonic' refers to wavelike disturbances with wavelength greater than that of the base wave and it contrasts with 'superharmonic' which refers to disturbances of wavelength equal to that of the base wave. Following earlier work by Longuet-Higgins (1978) and Tanaka (1983), Saffman (1985) showed that gravity waves are superharmonically unstable if their amplitude is sufficiently large.

In the presence of surface tension, and with gravity absent, Crapper (1957) found an exact solution of the full Euler equations that describes capillary waves on water of infinite depth for an irrotational flow. The exact solution describes a branch of travelling waves that bifurcates from the state in which the free surface of the water is flat and continues up to the point where the wave amplitude becomes large and the wave profiles feature a trapped air bubble. Recently Hur & Wheeler (2020) made the remarkable observation that the wave profiles described by Crapper's solution also describe travelling-waves on water of infinite depth in the absence of surface tension and gravity but in the presence of a background flow with constant shear. More specifically, Hur & Wheeler constructed a new exact solution to the background shear problem for which the surface wave profiles coincide exactly with those described by Crapper's solution but with a different flow field in the fluid. Their result followed earlier numerical work by Vanden-Broeck (1996), and later by Dyachenko & Hur (2019*a*), Dyachenko & Hur (2019*b*) and Hur & Vanden-Broeck (2020); in the latter three papers they showed that the wave profiles closely resemble those for the Crapper problem.

† Email address for correspondence: m.blyth@uea.ac.uk

The stability of the capillary waves described by Crapper's solution was first investigated by Chen & Saffman (1985) for small amplitude subharmonic perturbations and by Hogan (1988) for superharmonic perturbations. Hogan calculated linear growth rates for a range of wave amplitudes even up to that corresponding to the trapped-bubble profile, but his conclusion that large amplitude waves are superharmonically unstable is inconsistent with the later findings of Tiron & Choi (2012) who were able to achieve more accurate numerical computations. In fact Tiron & Choi (2012) showed that Crapper waves are superharmonically stable but subharmonically unstable over the whole amplitude range of Crapper's solution, the latter being consistent with the earlier small amplitude results of Chen & Saffman (1985).

In the present paper we examine the stability of the travelling waves described by Hur & Wheeler (2020) for the constant background shear problem. The effects of gravity and surface tension are both neglected. Although the surface profiles coincide with those for the Crapper solution, the dynamical problems are clearly different and the stability properties of the two problems are not expected to be the same. By extending the approach of Dyachenko *et al.* (1996), Choi (2009) reformulated the fully nonlinear background shear problem with gravity included in terms of surface variables only and demonstrated the presence of Benjamin-Feir instability via the solution of an initial value problem. Later Murashige & Choi (2020) presented an extensive study of the same gravity-shear problem using an alternative surface variables formulation. They found that, as for pure gravity waves, the system is subharmonically unstable and superharmonic instability may be triggered at sufficiently high amplitude depending on the sign and strength of the background shear.

In the next section we formulate the problem in the presence of a constant background shear flow on fluid of infinite depth using the surface-variable formulation of Choi (2009). In section 3 we discuss the base waves described by the exact solution due to Hur & Wheeler (2020). In section 4 we present a linear stability analysis for small amplitude base waves, and in section 5 we present numerical results for waves of finite amplitude. Finally in section 6 we summarise our findings.

2. Problem statement

We examine the stability of waves on fluid of infinite depth in the presence of a background linear shear current of constant strength $\omega > 0$. The base waves of wavelength $2\pi/k$ are assumed to be travelling with constant speed $c > 0$ in the positive x direction. Following Murashige & Choi (2020) it is convenient to formulate the mathematical problem in a frame of reference that is travelling at the basic wave speed c. In this case the condition

$$(u, v) \sim -(c + \omega y, 0) \tag{2.1}$$

as $y \to -\infty$ holds, where u and v are the velocity components in the x and y directions respectively.

With reference to a streamfunction $\bar{\psi}$ defined so that $u = \bar{\psi}_y$ and $v = -\bar{\psi}_x$, we have the relation $\nabla^2\bar{\psi} = -\omega$. It is convenient to introduce the shifted streamfunction ψ defined so that

$$\psi(x, y, t) = \bar{\psi}(x, y, t) + \tfrac{1}{2}\omega y^2, \tag{2.2}$$

in which case ψ is a harmonic function with $\nabla^2\psi = 0$. We also introduce the conjugate harmonic function ϕ which, together with ψ, satisfies the Cauchy-Riemann relations

$\phi_x = \psi_y$ and $\phi_y = -\psi_x$. The unsteady flow problem is then to solve

$$\nabla^2 \phi = 0 \tag{2.3}$$

in the fluid subject to the far-field condition

$$\nabla\phi \to -(c, 0) \quad \text{as } y \to -\infty. \tag{2.4}$$

Writing $(\tilde{x}(\xi, t), \tilde{y}(\xi, t))$ for a point on the free surface for real parameter ξ, we also have the kinematic condition,

$$(\tilde{x}_t + \omega\tilde{y} - \phi_x)n_x + (\tilde{y}_t - \phi_y)n_y = 0, \tag{2.5}$$

where (n_x, n_y) is the unit normal to the free surface and the partial derivatives are evaluated at the free surface. Finally we have the dynamic condition at the free surface that derives from the Bernoulli equation,

$$\phi_t + \frac{1}{2}|\nabla\phi|^2 + \omega\psi - \omega\tilde{y}\phi_x = B(t), \tag{2.6}$$

where the arbitrary function $B(t)$ can be incorporated into ϕ.

We make all variables dimensionless by referring them to the length and time scales k^{-1} and $(kc)^{-1}$ respectively. This is done implicitly in what follows. In so doing we introduce the dimensionless parameter,

$$\Omega = \frac{\omega}{kc}. \tag{2.7}$$

We make use of the conformal mapping technique that was introduced by Dyachenko *et al.* (1996), and which has been used by many subsequent authors, to reformulate the problem (2.3)-(2.6) as a pair of partial differential equations written in terms of surface variables only. The flow domain in the physical $x+\mathrm{i}y$ plane is mapped into the lower-half mapped plane $\xi + \mathrm{i}\eta$ with the free surface located at $\eta = 0$. Writing $\hat{\phi}(\xi, \eta, t) = \phi(x, y, t)$ and $\hat{\psi}(\xi, \eta, t) = \psi(x, y, t)$, under the conformal map $x = x(\xi, \eta, t)$, $y = y(\xi, \eta, t)$ we introduce the surface variables

$$\tilde{\phi}(\xi, t) = \hat{\phi}(\xi, 0, t), \qquad \tilde{\psi}(\xi, t) = \hat{\psi}(\xi, 0, t) \tag{2.8}$$

and

$$\tilde{x}(\xi, t) = x(\xi, 0, t), \qquad \tilde{y}(\xi, t) = y(\xi, 0, t). \tag{2.9}$$

After some working we obtain the governing equations

$$\tilde{\phi}_t = -\frac{1}{2J}\left(\tilde{\phi}_\xi^2 - \tilde{\psi}_\xi^2\right) + \tilde{\phi}_\xi \mathcal{H}\left[\frac{\tilde{\psi}_\xi}{J}\right] + \Omega\left(\tilde{\phi}_\xi\left(\frac{\tilde{y}\tilde{x}_\xi}{J} - \mathcal{H}\left[\frac{\tilde{y}\tilde{y}_\xi}{J}\right]\right) - \tilde{\psi}\right) + B(t), \tag{2.10}$$

and

$$\tilde{y}_t = \tilde{y}_\xi \mathcal{H}\left[\frac{\tilde{\psi}_\xi}{J}\right] - \tilde{x}_\xi \frac{\tilde{\psi}_\xi}{J} + \Omega\, \tilde{y}_\xi\left(\frac{\tilde{y}\tilde{x}_\xi}{J} - \mathcal{H}\left[\frac{\tilde{y}\tilde{y}_\xi}{J}\right]\right), \tag{2.11}$$

where $J = \tilde{x}_\xi^2 + \tilde{y}_\xi^2$, together with the additional relationships

$$\tilde{x}_\xi = 1 - \mathcal{H}[\tilde{y}_\xi], \qquad \tilde{\phi}_\xi = -1 - \mathcal{H}\left[\tilde{\psi}_\xi\right]. \tag{2.12}$$

The Hilbert transform is defined in terms of a Cauchy principal value integral as

$$\mathcal{H}[f](x) = \frac{1}{\pi}\fint_{-\infty}^{\infty} \frac{f(x')}{x' - x}\, dx', \tag{2.13}$$

and it has the property that $\mathcal{H}[\mathcal{H}[f]] = -f$.

3. Travelling-wave solutions

For steadily propagating fixed form waves we have $\tilde{\phi}_t = 0 = \tilde{y}_t$ and B constant. Substituting (2.11) into (2.10), and using (2.12) and the fact that $\tilde{\psi}_\xi = \Omega\tilde{y}\tilde{y}_\xi$ from the non-dimensionalised form of (2.2) evaluated at the surface, after some manipulation we obtain

$$\frac{1}{2J}\Big(\Omega\mathcal{H}[Y_0Y_{0\xi}] + \Omega Y_0X_{0\xi} + 1\Big)^2 = C \tag{3.1}$$

where we have written $\tilde{x} = X_0(\xi)$ and $\tilde{y} = Y_0(\xi)$, and where $C = B - \Omega\bar{\psi}$ with $\bar{\psi}$ taking its constant value on the free surface. Remarkably, Hur & Wheeler (2020) have recently given an exact solution to this problem whose surface wave profiles correspond exactly to those described by the exact solution of Crapper (1957) for pure capillary waves on deep water. However, the flow fields differ between the two problems. The free surface is given by

$$X_0 + \mathrm{i}Y_0 = \xi - \frac{4\mathrm{i}A\mathrm{e}^{-\mathrm{i}\xi}}{1 + A\mathrm{e}^{-\mathrm{i}\xi}}, \tag{3.2}$$

where A is a real parameter such that

$$A^2 = \frac{1-\Omega}{1-3\Omega} \qquad \text{or} \qquad \Omega = \frac{1-A^2}{1-3A^2}, \tag{3.3}$$

and, for physically acceptable (i.e. non self-intersecting) solutions $A \in [0, A^*]$ or $\Omega \in [1, \Omega^*]$ with $A^* = 0.4547$ and $\Omega^* = 2.0885$. Wave overturning occurs for $A > \tilde{A}$ where $\tilde{A} = \sqrt{2} - 1 \approx 0.4142$. A number of travelling wave profiles are plotted in Figure 1 together with a bifurcation diagram showing where the travelling-wave branch bifurcates from the flat state at $\Omega = 1$.

The steady forms of $\tilde{\psi}$ and $\tilde{\phi}$ corresponding to (3.2) are

$$\tilde{\psi} = \Psi_0(\xi) = \frac{1}{2}\Omega Y_0^2, \qquad \tilde{\phi} = \Phi_0(\xi) = -\xi - \tfrac{1}{2}\Omega\mathcal{H}\big[Y_0^2\big]\,. \tag{3.4}$$

4. Linear stability analysis

We carry out a linear stability analysis by perturbing the basic state, writing

$$\tilde{x} = X_0(\xi) + X_1(\xi, t), \quad \tilde{y} = Y_0(\xi) + Y_1(\xi, t), \tag{4.1}$$

and

$$\tilde{\phi} = \Phi_0(\xi) + \Phi_1(\xi, t), \quad \tilde{\psi} = \Psi_0(\xi) + \Psi_1(\xi, t), \tag{4.2}$$

where we assume that $|X_1| \ll |X_0|$ etc. (It is not necessary to perturb the Bernoulli constant since any such perturbation can be absorbed into the perturbation for $\tilde{\phi}$.) In what follows the basic state is taken to be either that for which the free surface is flat or for which it exhibits one of the travelling-wave solutions described in section 3.

Substituting (4.1) into (2.10), and then linearising and simplifying using (3.4), we

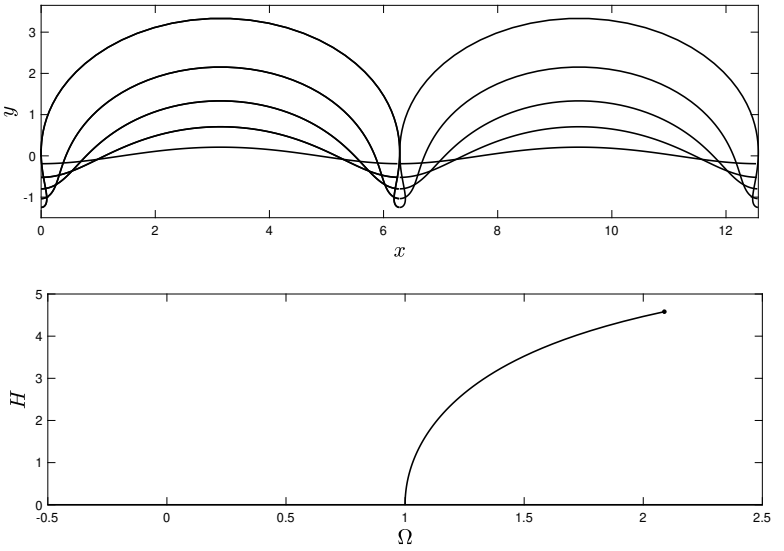

Figure 1: Upper: travelling wave profiles (X_0, Y_0) given by (3.2) for the values $(A, \Omega) = (0.05, 1.005)$, $(0.15, 1.048)$, $(0.25, 1.154)$, $(0.35, 1.387)$ and (A^*, Ω^*), where $A^* = 0.4547$ and $\Omega^* = 2.089$. Lower: the solution branch corresponding to the travelling waves (X_0, Y_0) shown in the upper panel, with the wave height $H = \max Y_0 - \min Y_0$. The branch bifurcates from the flat state ($A = 0$), which exists for all Ω, at $\Omega = 1$. The filled circle at $\Omega = \Omega^* = 2.09$, $H = 4.48$ indicates where the wave profiles start to self-intersect.

obtain

$$\Phi_{1t} = \left(\frac{J_1}{2J_0^2} \left(\Phi_{0\xi}^2 - \Psi_{0\xi}^2 \right) - \frac{1}{J_0} \left(\Phi_{0\xi}\Phi_{1\xi} - \Psi_{0\xi}\Psi_{1\xi} \right) \right) + \Phi_{0\xi}\mathcal{H}\left[\frac{\Psi_{1\xi}}{J_0} \right]$$
$$+ \Omega \left(\Phi_{1\xi} \frac{Y_0 X_{0\xi}}{J_0} + \Phi_{0\xi} \frac{Y_1 X_{0\xi}}{J_0} + \Phi_{0\xi} \frac{Y_0 X_{1\xi}}{J_0} - \Phi_{0\xi} J_1 \frac{Y_0 X_{0\xi}}{J_0^2} - \Phi_{0\xi}\mathcal{H}\left[\frac{Y_1 Y_{0\xi}}{J_0} \right] \right.$$
$$\left. - \Phi_{0\xi}\mathcal{H}\left[\frac{Y_0 Y_{1\xi}}{J_0} \right] - \Psi_1 \right), \tag{4.3}$$

where $J_0 = X_{0\xi}^2 + Y_{0\xi}^2$ and $J_1 = 2\big(X_{0\xi}X_{1\xi} + Y_{0\xi}Y_{1\xi}\big)$. Substituting (4.1) into (2.11), and linearising, we find

$$Y_{1t} = Y_{0\xi}\mathcal{H}\left[\frac{\Psi_{1\xi}}{J_0} \right] - X_{0\xi} \frac{\Psi_{1\xi}}{J_0}$$
$$+ \Omega \left(X_{0\xi} \frac{Y_1 Y_{0\xi}}{J_0} + X_{0\xi} \frac{Y_0 Y_{1\xi}}{J_0} - Y_{0\xi}\mathcal{H}\left[\frac{Y_1 Y_{0\xi}}{J_0} \right] - Y_{0\xi}\mathcal{H}\left[\frac{Y_0 Y_{1\xi}}{J_0} \right] \right). \tag{4.4}$$

The linearised relationships (2.12) are

$$X_{1\xi} = -\mathcal{H}[Y_{1\xi}], \qquad \Phi_{1\xi} = -\mathcal{H}[\Psi_{1\xi}]. \tag{4.5}$$

To investigate the stability of the spatially-periodic travelling waves described in

section 3, we may appeal to Floquet theory to express the perturbations in the form

$$\boldsymbol{X} = \mathrm{e}^{\sigma t}\mathrm{e}^{\mathrm{i}p\xi}\sum_{n=-\infty}^{\infty}\boldsymbol{\alpha}_n\mathrm{e}^{\mathrm{i}n\xi}, \tag{4.6}$$

where $\boldsymbol{X} = (X_1, Y_1, \Phi_1, \Psi_1)^T$ and $\boldsymbol{\alpha}_n = (a_n, b_n, c_n, d_n)^T$ is a constant vector. Here $\sigma \in \mathbb{C}$ is the complex growth rate, which is to be determined, and $p \in [0, 1)$ is a chosen parameter. If $\mathrm{Re}(\sigma) > 0$ then the flow is unstable. When $p = 0$ the perturbation corresponds to a superharmonic disturbance, and when $0 < p < 1$ the perturbation corresponds to a subharmonic disturbance.

We note that

$$\mathcal{H}\big[\mathrm{e}^{\mathrm{i}q\xi}\big] = \mathrm{i}\,\mathrm{sgn}(q)\mathrm{e}^{\mathrm{i}q\xi} \tag{4.7}$$

for any $q \in \mathbb{R}$. Substituting (4.6) into (4.5) we find that if $n + p \neq 0$

$$\mathrm{i}a_n = \mathrm{sgn}(n+p)b_n, \qquad \mathrm{i}c_n = \mathrm{sgn}(n+p)d_n, \tag{4.8}$$

which allows us to eliminate, for example, a_n and d_n from the problem. Furthermore if $\{\sigma, p, b_n, c_n\}$ is an eigenset then so is

$$\{\sigma^*, -p, b^*_{-n}, c^*_{-n}\},$$

where an asterisk denotes a complex conjugate. This can be seen by substituting (4.6) into (4.3) and (4.4), conjugating the resulting equations, and then making the transformation $(n, p) \mapsto (-n, -p)$. A similar symmetry was noted by Tiron & Choi (2012) for the stability problem associated with capillary waves on water of infinite depth; see also Blyth & Părău (2016) for capillary waves on fluid sheets. Again similar to Tiron & Choi's case we note that

$$\{-\sigma, -p, b_{-n}, -c_{-n}\} \qquad \text{and} \qquad \{-\sigma^*, p, b^*_{-n}, -c^*_{-n}\}$$

are both eigensets. These symmetries allow us to restrict attention to the set $p \in [0, 1/2]$.

For superharmonic waves with $p = 0$, the translational symmetry of the problem implies that, for any amplitude A, $\boldsymbol{X} = (X_{0\xi}, Y_{0\xi}, \Phi_{0\xi}\ \Psi_{0\xi})^T$ is an eigenfunction for the zero eigenvalue. Moreover, the symmetries just noted imply that this zero eigenvalue has algebraic multiplicity four.

4.1. *Stability in the limit of zero amplitude*

The amplitude of the waves approaches zero as $\Omega \to 1$. In this limit we attain the flat surface state

$$X_0 = \xi, \qquad Y_0 = 0, \qquad \Psi_0 = 0, \qquad \Phi_0 = -\xi.$$

Equations (4.3) and (4.4) reduce to (with $\Omega = 1$)

$$\Phi_{1t} = X_{1\xi} + \Phi_{1\xi} - \mathcal{H}[\Psi_{1\xi}] - Y_1 - \Psi_1, \qquad Y_{1t} = -\Psi_{1\xi}. \tag{4.9}$$

respectively. Inserting the ansatz (4.6) the complex growth rate satisfies the quadratic equation

$$\sigma^2 + \mathrm{i}\big(\mathrm{sgn}(n+p) - 2(n+p)\big)\sigma + |n+p| - |n+p|^2 = 0, \tag{4.10}$$

for integer n. Then

$$\sigma_{\mathrm{I}}(n; p) = \mathrm{i}(n+p), \qquad \sigma_{\mathrm{II}}(n; p) = \mathrm{i}(n+p) - \mathrm{i}\,\mathrm{sgn}(n+p). \tag{4.11}$$

All of the eigenvalues lie on the imaginary axis and each has multiplicity at least two. For superhamonic perturbations with $p = 0$ we have the set of double eigenvalues

$$\mathrm{i}n = \sigma_{\mathrm{I}}(n;0) = \sigma_{\mathrm{II}}(n + \mathrm{sgn}(n);0) \qquad (n \neq 0), \tag{4.12}$$

and the quadruple zero eigenvalue

$$0 = \sigma_{\mathrm{I}}(0;0) = \sigma_{\mathrm{II}}(0;0) = \sigma_{\mathrm{II}}(1;0) = \sigma_{\mathrm{II}}(-1;0). \tag{4.13}$$

For subharmonic perturbations, $p \in (0,1)$, we have the set of double eigenvalues

$$\mathrm{i}(n+p) = \sigma_{\mathrm{I}}(n;p) = \sigma_{\mathrm{II}}(n + \mathrm{sgn}(n+p);p) \qquad (n \notin \{0,-1\}), \tag{4.14}$$

and the set of triple eigenvalues

$$\mathrm{i}(n+p) = \sigma_{\mathrm{I}}(n;p) = \sigma_{\mathrm{II}}(n+1;p) = \sigma_{\mathrm{II}}(n-1;p) \qquad (n \in \{0,-1\}). \tag{4.15}$$

4.2. *Stability of small amplitude waves*

We now examine the stability of the base waves of small amplitude with $A \ll 1$. Expanding (3.2) for small A we have

$$X_0(\xi) = \xi + AX_{01}(\xi) + O(A^2), \qquad Y_0(\xi) = AY_{01}(\xi) + O(A^2), \tag{4.16}$$

where $X_{01} = -4\sin\xi$ and $Y_{01} = -4\cos\xi$. From (3.3) $\Omega = 1 + 2A^2 + O(A^4)$, and from (3.4) $\Psi_{0\xi} = \Omega Y_0 Y_{0\xi} = O(A^2)$ and $\Phi_{0\xi} = -1 + O(A^2)$.

We assume that

$$(X_1,\, Y_1,\, \Phi_1,\, \Psi_1)^T = \mathrm{e}^{\sigma t}\boldsymbol{u}, \tag{4.17}$$

where $\boldsymbol{u} = \boldsymbol{u}(\xi)$. Substituting into (4.3) and (4.4), and using (4.5), we obtain the linear system

$$\boldsymbol{L}\boldsymbol{u} = \sigma\boldsymbol{u}, \tag{4.18}$$

where $\boldsymbol{L}$ is a differential operator that depends on the amplitude A. We expand by writing

$$\boldsymbol{L} = \boldsymbol{L}_0 + A\boldsymbol{L}_1 + \cdots, \qquad \boldsymbol{u} = \boldsymbol{u}_0 + A\boldsymbol{u}_1 + \cdots, \qquad \sigma = \sigma_0 + A\sigma_1 + \cdots. \tag{4.19}$$

Substituting (4.19) into (4.18), at leading order

$$\boldsymbol{L}_0\boldsymbol{u}_0 = \sigma_0\boldsymbol{u}_0. \tag{4.20}$$

The explicit form of $\boldsymbol{L}_0$ is given in Appendix A; we shall henceforth refer to it as the flat state operator. At first order,

$$(\boldsymbol{L}_0 - \sigma_0\boldsymbol{I})\boldsymbol{u}_1 = -(\boldsymbol{L}_1 - \sigma_1\boldsymbol{I})\boldsymbol{u}_0, \tag{4.21}$$

where $\boldsymbol{I}$ is the identity operator, and the explicit form of $\boldsymbol{L}_1$ is given in Appendix A. Assuming that σ_0 is an eigenvalue of $\boldsymbol{L}_0$ according to (4.20), the first order problem (4.21) has a solution if and only if the right hand side satisfies one or more solvability conditions according to the Fredholm alternative (e.g. Kapitula & Promislow 2013). The latter requires that the right hand side of (4.21) be orthogonal to the nullspace of the adjoint of the operator on the left hand side. Suppose that $\boldsymbol{v}_0$ satisfies

$$(\boldsymbol{L}_0^\dagger - \sigma_0^*\boldsymbol{I})\boldsymbol{v}_0 = 0, \tag{4.22}$$

where $\boldsymbol{L}_0^\dagger$ is the adjoint of $\boldsymbol{L}_0$ defined such that $\langle \boldsymbol{L}\boldsymbol{f}, \boldsymbol{g}\rangle = \langle \boldsymbol{f}, \boldsymbol{L}^\dagger\boldsymbol{g}\rangle$, and the inner product is

$$\langle \boldsymbol{a}, \boldsymbol{b}\rangle = \frac{1}{2\pi}\int_0^{2\pi} (\boldsymbol{a}^*)^T\boldsymbol{b}\, d\xi. \tag{4.23}$$

The kernel of the adjoint operator $\boldsymbol{L}_0^\dagger - \sigma_0^* \boldsymbol{I}$ has dimension greater than unity, a point that is suggested by the multiplicities of the flat-state eigenvalues noted in section 4.1. We consider the following cases specific to the imaginary double and triple eigenvalues identified for the flat state in section 4.1.

4.2.1. *Double eigenvalues*

According to (4.12) and (4.14), the flat state operator $\boldsymbol{L}_0$ has the double eigenvalue $\sigma_0 = \mathrm{i}(n+p)$ if $p = 0$ and $n \neq 0$, or if $p \neq 0$ and $n \notin \{0, -1\}$. In this case the kernel of $\boldsymbol{L}_0 - \sigma_0 \boldsymbol{I}$ has two basis vectors, for example

$$\boldsymbol{e}_1 = \boldsymbol{\alpha}_1 \, \mathrm{e}^{\mathrm{i}(n+p)\xi}, \qquad \boldsymbol{e}_2 = \boldsymbol{\alpha}_2 \, \mathrm{e}^{\mathrm{i}(n+p+s)\xi}, \tag{4.24}$$

where $s = \mathrm{sgn}(n+p)$, with

$$\boldsymbol{\alpha}_1 = (s\mathrm{i}, \, -1, \, -s\mathrm{i}, \, 1)^T, \qquad \boldsymbol{\alpha}_2 = \left(\frac{n\mathrm{i}}{n+s}, \, -\frac{n}{n+s}, \, -s\mathrm{i}, \, 1 \right)^T.$$

The kernel of $\boldsymbol{L}_0^\dagger - \sigma_0^* \boldsymbol{I}$ has a basis with spanning set $\{\boldsymbol{e}_1', \boldsymbol{e}_2'\}$ with corresponding definitions to (4.24), and

$$\boldsymbol{\alpha}_1' = (n\mathrm{i}, \, 0, \, n\mathrm{i}, \, 1)^T, \qquad \boldsymbol{\alpha}_2' = ((n+s)\mathrm{i}, \, 0, \, (n+s)\mathrm{i}, \, 1)^T.$$

The required solvability conditions are (with $k = 2$ in this case)

$$\sum_{i=1}^{k} a_i \langle \boldsymbol{e}_j', \, (\boldsymbol{L}_1 - \sigma_1 \boldsymbol{I}) \boldsymbol{e}_i \rangle = 0, \tag{4.25}$$

for $j = 1, 2$, where $a_i = \langle \boldsymbol{e}_i, \boldsymbol{u}_0 \rangle$. These conditions are conveniently rewritten as

$$\boldsymbol{M}\boldsymbol{a} = \sigma_1 \boldsymbol{a}, \tag{4.26}$$

where $\boldsymbol{a} = (a_1, a_2)^T$ and the elements of the matrix $\boldsymbol{M}$ are

$$M_{ij} = \mu_i^{-1} \langle \boldsymbol{e}_i', \, \boldsymbol{L}_1 \boldsymbol{e}_j \rangle, \tag{4.27}$$

where $\mu_j = \langle \boldsymbol{e}_j', \, \boldsymbol{e}_j \rangle$. Hence

$$\sigma_1 = \pm \left(\frac{\langle \boldsymbol{e}_1', \, \boldsymbol{L}_1 \boldsymbol{e}_2 \rangle \langle \boldsymbol{e}_2', \, \boldsymbol{L}_1 \boldsymbol{e}_1 \rangle}{\langle \boldsymbol{\alpha}_1', \, \boldsymbol{\alpha}_1 \rangle \langle \boldsymbol{\alpha}_2', \, \boldsymbol{\alpha}_2 \rangle} \right)^{1/2}. \tag{4.28}$$

This reduces to

$$\sigma_1 = \pm 2 \sqrt{(n+p)(n+p+\mathrm{sgn}(n+p))} \in \mathbb{R} \tag{4.29}$$

which holds if $p = 0$ and $n \neq 0$, or if $p \neq 0$ and $n \notin \{0, -1\}$. Evidently the waves on the bifurcation branch in Figure 1 are unstable for any $A > 0$.

4.2.2. *Triple eigenvalues*

The flat state operator $\boldsymbol{L}_0$ has the pair of triple eigenvalues $\sigma_0 = \mathrm{i}p$ and $\sigma_0 = \mathrm{i}(-1+p)$ with $p \neq 0$ (see 4.15). For the eigenvalue $\sigma = \mathrm{i}p$ the kernel of $\boldsymbol{L}_0 - \mathrm{i}p\boldsymbol{I}$ has the basis vectors

$$\boldsymbol{e}_1 = \boldsymbol{\beta}_1 \mathrm{e}^{\mathrm{i}p\xi}, \qquad \boldsymbol{e}_2 = \boldsymbol{\beta}_2 \mathrm{e}^{\mathrm{i}(p+1)\xi}, \qquad \boldsymbol{e}_3 = \boldsymbol{\beta}_3 \mathrm{e}^{\mathrm{i}(p-1)\xi}, \tag{4.30}$$

with

$$\boldsymbol{\beta}_1 = (\mathrm{i}, \, -1, \, -\mathrm{i}, \, 1)^T, \quad \boldsymbol{\beta}_2 = \left(\frac{p\mathrm{i}}{p+1}, \, -\frac{p}{p+1}, \, -\mathrm{i}, \, 1 \right)^T, \quad \boldsymbol{\beta}_3 = \left(\frac{p\mathrm{i}}{1-p}, \, \frac{p}{1-p}, \, \mathrm{i}, \, 1 \right)^T.$$

The kernel of the adjoint operator $\boldsymbol{L}_0^\dagger + \mathrm{i}p\boldsymbol{I}$ has basis vectors with definitions corresponding to (4.30) and with

$$\boldsymbol{\beta}_1' = (p\mathrm{i},\, 0,\, p\mathrm{i},\, 1)^T, \quad \boldsymbol{\beta}_2' = ((p+1)\mathrm{i},\, 1,\, (p+1)\mathrm{i},\, 1)^T, \quad \boldsymbol{\beta}_3' = ((p-1)\mathrm{i},\, 1,\, (p-1)\mathrm{i},\, 1)^T.$$

The required solvability conditions are given by (4.25) with $k = 3$ for $j = 1, 2, 3$. In this case the matrix $\boldsymbol{M}$ in (4.26) is 3×3 and has the elements given in (4.27). Solving for the eigenvalues of $\boldsymbol{M}$ we find after a little algebra that

$$\sigma_1 = \pm 2\sqrt{2}p \qquad \text{and} \qquad \sigma_1 = 0. \tag{4.31}$$

For the eigenvalue $\sigma_0 = \mathrm{i}(-1 + p)$ the details are similar. In this case the solvability conditions yield

$$\sigma_1 = \pm 2\sqrt{2}(p-1) \qquad \text{and} \qquad \sigma_1 = 0, \tag{4.32}$$

implying instability.

5. Numerical calculations

We compute the eigenvalues σ numerically. We truncate the infinite series in (4.6) at $n = \pm N$, for some integer N, and substitute into (4.3) and (4.4). Next we introduce the grid of collocation points $\xi_k = 2\pi(k-1)/M$, for $k = 1, \cdots, M$, where $M = 4N + 2$, and evaluate the equations at each collocation point in turn to yield M algebraic equations for the M unknown coefficients b_n, c_n (we use (4.8) to eliminate a_n and d_n). We then write these equations in the form

$$\sigma \boldsymbol{A}\boldsymbol{x} = \boldsymbol{B}\boldsymbol{x}, \tag{5.1}$$

where $\boldsymbol{x} = (b_{-N}, \ldots, b_N, c_{-N}, \ldots, c_N)^T$. In numerical practice we calculate the $M \times M$ matrices $\boldsymbol{A}$, $\boldsymbol{B}$ using the method of impulses: we set $\boldsymbol{x} = \boldsymbol{e}_i$, where $\boldsymbol{e}_i$ is the zero vector with its ith zero replaced by unity, and then compile column by column by taking $i = 1, \cdots, M$. We solve the generalised eigenproblem using the Matlab inbuilt function *eig* which implements the QZ algorithm.

For superharmonic perturbations, $p = 0$, we find numerically that there are four zero eigenvalues for any amplitude $A > 0$ in agreement with expectation (see section 4). In Figure 2 we show the growth rates σ in the complex plane for two values of the amplitude parameter A. The empty circles indicate the eigenvalues for the superharmonic case $p = 0$. Varying p continuously in the range $[0, 1)$ traces a continuous line (shown as a solid blue line in the figure) that connects pairs of empty circles. The arrows indicate how the simple $p = 0$ eigenvalues (empty circles) have split from their double eigenvalue counterparts that exist for $A = 0$ on the imaginary axis, and which are shown with a $\otimes$ symbol. In fact all of the double eigenvalues that exist at $A = 0$, namely $\sigma = \mathrm{i}(n + p)$ for $|n| \geqslant 1$, split for $A > 0$, sliding right and left into the complex plane as A increases according to the theory of section 4.2.1. The theoretical prediction for the eigenvalues up to first order in A – see (4.19), (4.29) – is superimposed on the numerical results in the figure (shown as filled triangles) with excellent agreement. The triple eigenvalues at $A = 0$, namely $\sigma = \mathrm{i}p$ and $\sigma = \mathrm{i}(-1 + p)$ (not shown in the figure), divide for $A > 0$ and the three split eigenvalues slide along the imaginary axis and left/right into the complex plane according to the theory in section 4.2.2. The theoretical prediction up to first order in A, given by (4.19) and (4.31), is shown in the figure with filled circles with excellent agreement. The agreement between the theory and the numerics deteriorates at larger n, the divergence appearing earlier for larger A (see the right-hand panel).

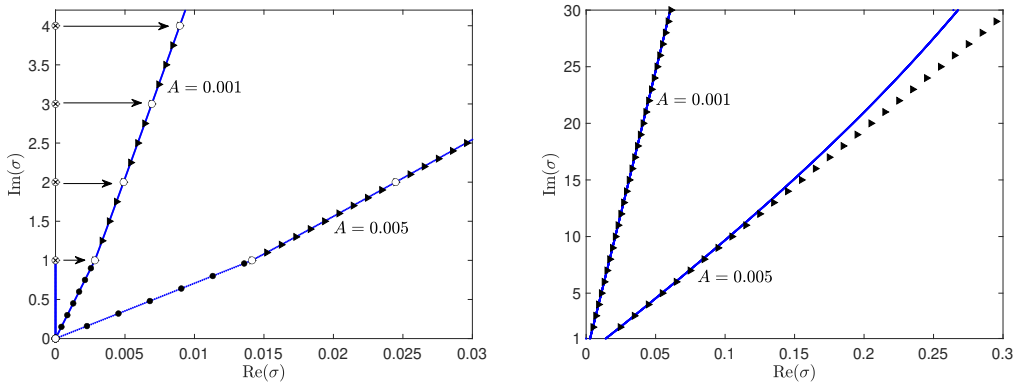

Figure 2: The numerically computed complex growth rate, σ, shown with blue solid lines for $A = 0.001$ and $A = 0.005$ and $p \in [0, 1)$. The theoretical predictions $\sigma_0 + A\sigma_1$, with $\sigma_0 = \mathrm{i}(n + p)$ ($n \in \mathbb{Z}$) and σ_1 given by (4.29) and (4.31) are shown with solid triangles and solid circles, respectively. The other symbols and annotations are explained in the text. Only the first quadrant of the complex σ plane is shown; the remainder can be constructed by symmetry. The left panel shows results closer to the origin than the right panel.

The splitting of the double and triple eigenvalues is illustrated more clearly in Figure 3. In particular, the typical double eigenvalue $\sigma = \mathrm{i}$ is shown to split as A increases from zero, the divided eigenvalues forming a conjugate pair that moves off the imaginary axis into the complex plane. The typical triple eigenvalue $\sigma = \mathrm{i}p$ for $p = 0.2$ splits for $A > 0$ into a conjugate pair and an imaginary eigenvalue that moves up the imaginary axis as A increases. The predictions from the theory presented in sections 4.2.1 and 4.2.2 are also shown, and the agreement with the numerical computations is seen to be excellent for sufficiently small A but to worsen as A increases in line with expectations.

The complex growth rates for larger values of A are shown in Figure 4. This includes stability results for an overturning base wave with $A = 0.43$ (recall that wave overturning occurs for $A > \tilde{A} \approx 0.4142$). As in Figure 4 the empty circles indicate the eigenvalues for $p = 0$. Varying p in the range $[0, 1)$ fills the spaces along the curves between the white circles. In each case the eigenvalues have split from their base state counterparts at $A = 0$ on the imaginary axis in the manner described above. The departure from the small amplitude theory of section 4.2, which suggests that the real part of the growth rates should increase roughly linearly with n (for fixed p), is more evident here. In particular, the growth rate curves for $A = 0.025$ (left panel) form a figure-eight structure, which is reminiscent of that seen in other wave stability studies; see, for example, the gravity water wave computations of Deconinck & Oliveras (2011), Deconinck & Trichtchenko (2014) and Akers & Nicholls (2012), to name just a few. It should be emphasised however, that the formation of the figure eight is different between the present case and the aforementioned studies. In the latter the entire figure-eight curve is obtained by varying p over the range $[0, 1)$. In our case, the superhamonic values $p = 0$ correspond to a set of points distributed around the figure eight (shown as empty circles in the figure), and varying p over the range $[0, 1)$ simultaneously fills the individual segments that connect these $p = 0$ eigenvalues. Immediately above the figure-eight curve there is a short interval of purely imaginary eigenvalues (seen in the close-up inset in the left panel) that are distinct from the purely imaginary eigenvalues at $A = 0$ discussed in section 4.

The right panel of Figure 4 shows how the pinched figure-eight structure splits and

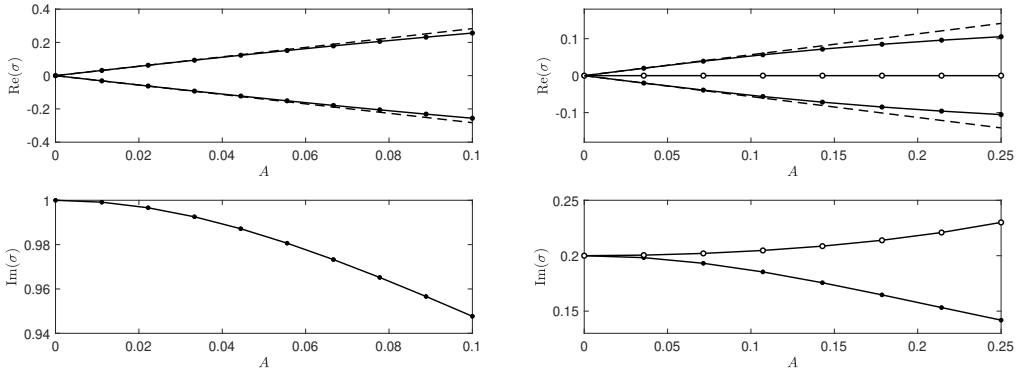

Figure 3: Left panel: the double eigenvalue $\sigma = \mathrm{i}$ for $p = 0$, shown as a solid line with dots, splits into two as A increases; the broken lines in the upper left panel follow the theoretical prediction $\mathrm{Re}(\sigma) = \pm 2\sqrt{2}A$ according to (4.29). Note that the imaginary parts of the split eigenvalues are the same. Right panel: the upper right panel shows how the triple eigenvalue $\sigma = \mathrm{i}p$ for $p = 0.2$ splits into three as A increases; the broken lines show the theoretical prediction $\mathrm{Re}(\sigma) = \pm 2\sqrt{2}pA$ according to (4.31). Note that the imaginary parts of the split eigenvalues with non-zero real part (shown as a solid line with filled circles) are the same. The solid line with empty circles in the lower right panel shows the imaginary part of the split eigenvalue with zero real part.

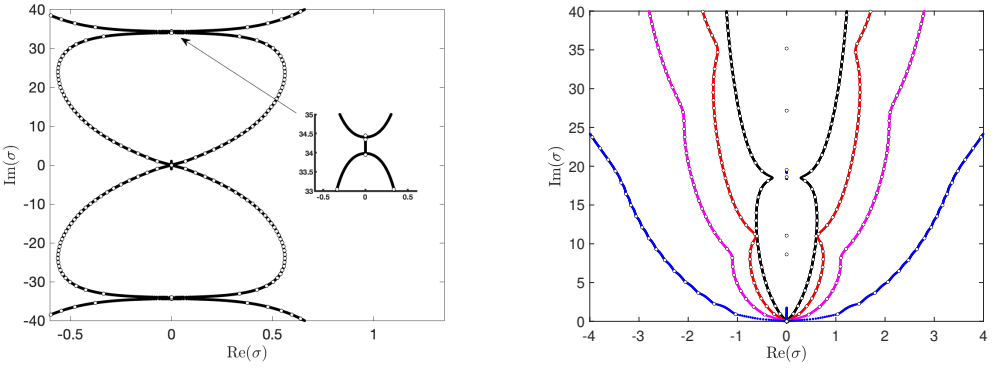

Figure 4: The complex growth rate, σ, for various A over the range $p \in [0, 1)$. Values for $p = 0$ are shown with white disks. Left: $A = 0.025$ (the inset shows a close-up near to $\mathrm{Im}(\sigma) = 34$. Right: $A = 0.05$ (black), $A = 0.1$ (red), $A = 0.2$ (magenta) and $A = 0.43$ (blue).

opens outwards as A is increased toward the critical value $A^* \approx 0.45$ at which the base waves start to self-intersect. For each A there exist one or possibly more intervals of purely imaginary eigenvalues in each of which p takes values in the range $[0, 1)$.

6. Summary

We have carried out a linear stability analysis of the travelling-wave solutions found by Hur & Wheeler (2020) as an exact solution of the Euler equations for waves on an infinite depth fluid in the presence of a constant background shear field. The effects of gravity and of surface tension have both been neglected. We have shown that waves of any non-zero

amplitude are linearly unstable to both superharmonic and subharmonic perturbations. These results have been obtained through the use of an asymptotic expansion in the base wave amplitude and by numerical computations valid for travelling waves of arbitrary amplitude up to the point of self-intersection and including where the base waves are overturning.

Our findings are rather different to what is known for gravity waves, capillary waves, and gravity-capillary waves. Gravity waves are subharmonically unstable for small amplitude over a range of p values subtended from zero that extends as the amplitude increases (McLean 1982; Deconinck & Oliveras 2011); this is the Benjamin-Feir instability. The unstable p range detaches from zero at a certain amplitude (McLean 1982; Deconinck & Oliveras 2011). Gravity waves are superharmonically unstable at sufficiently large amplitude (Saffman 1985). Capillary waves are superharmonically stable at any amplitude, and are subharmonically unstable at any non-zero amplitude over a range of p values subtended from zero that extends as the amplitude increases as for gravity waves (Tiron & Choi 2012). Results for gravity-capillary waves for small surface tension are similar to those for gravity waves (Deconinck & Trichtchenko 2014). For the present problem, the waves are superharmonically unstable at any amplitude, and they are subharmonically unstable for any amplitude over the entire range of p values. We note that if gravity is included along with the background shear then subharmonic instability occurs only for certain values of p as is the case for pure gravity waves (Murashige & Choi 2020).

Declaration of Interests

The authors report no conflict of interest.

Appendix A. The operators $\boldsymbol{L}_0$ and $\boldsymbol{L}_1$

The flat state operator appearing in (4.20) is such that

$$\boldsymbol{L}_0\boldsymbol{u} \equiv \left(\boldsymbol{A}_0\frac{d}{d\xi} + \boldsymbol{B}_0\right)\boldsymbol{u} + \boldsymbol{C}_0\,\mathcal{H}[\boldsymbol{u}] + \boldsymbol{D}_0\mathcal{H}\left[\frac{d\boldsymbol{u}}{d\xi}\right], \tag{A 1}$$

where

$$\boldsymbol{A}_0 = \begin{pmatrix} 1 & 0 & 1 & 0, \\ 0 & 1 & 0 & 0 \\ 0 & 0 & 0 & 0 \\ 0 & -1 & 0 & 0 \end{pmatrix}, \qquad \boldsymbol{B}_0 = \begin{pmatrix} 0 & -1 & 0 & -1 \\ 0 & 0 & 0 & 0 \\ 0 & 0 & 0 & 0 \\ 0 & 0 & 0 & 0 \end{pmatrix}, \tag{A 2}$$

and

$$\boldsymbol{C}_0 = \begin{pmatrix} 0 & 0 & 0 & 0 \\ 0 & -1 & 0 & -1 \\ 0 & 0 & 0 & 0 \\ 0 & 0 & 0 & 0 \end{pmatrix} \qquad \boldsymbol{D}_0 = \begin{pmatrix} 0 & -1 & 0 & 0 \\ 1 & 0 & 1 & 0 \\ 0 & 1 & 0 & 0 \\ 0 & 0 & 0 & 0 \end{pmatrix}. \tag{A 3}$$

Its adjoint is such that

$$\boldsymbol{L}_0^{\dagger}\boldsymbol{u} \equiv -\boldsymbol{A}_0^{*}\boldsymbol{u}_{\xi} + \boldsymbol{B}_0^{*}\boldsymbol{u} - \mathcal{H}[\boldsymbol{C}_0^{*}\boldsymbol{u}] + \mathcal{H}\left[\boldsymbol{D}_0^{*}\frac{d\boldsymbol{u}}{d\xi}\right], \tag{A 4}$$

where the asterisk indicates the conjugate transpose.

The perturbation operator is defined such that

$$\boldsymbol{L}_1\boldsymbol{u} \equiv \left(\boldsymbol{A}_1\frac{d}{d\xi} + \boldsymbol{B}_1\right)\boldsymbol{u} + \mathcal{H}[\boldsymbol{C}_1\boldsymbol{u}] + \mathcal{H}\left[\boldsymbol{D}_1\frac{d\boldsymbol{u}}{d\xi}\right] + \boldsymbol{E}_1\mathcal{H}\left[\frac{d\boldsymbol{u}}{d\xi}\right]. \tag{A 5}$$

with

$$\boldsymbol{A}_1 = \begin{pmatrix} Y_{01} - 2X_{01\xi} & 0 & (Y_{01} - 3X_{01\xi}) & Y_{01\xi} \\ 0 & -2X_{01\xi} & 0 & -Y_{01} \\ 0 & Y_{01\xi} & 0 & 0 \\ 0 & X_{01\xi} & 0 & Y_{01} \end{pmatrix}, \tag{A 6}$$

and

$$\boldsymbol{B}_1 = \begin{pmatrix} 0 & 0 & 0 & X_{01\xi} \\ 0 & 0 & 0 & -Y_{01\xi} \\ 0 & 0 & 0 & 0 \\ 0 & 0 & 0 & Y_{01\xi} \end{pmatrix}, \qquad \boldsymbol{C}_1 = \begin{pmatrix} 0 & 0 & 0 & Y_{01\xi} \\ 0 & 0 & 0 & X_{01\xi} \\ 0 & 0 & 0 & -Y_{01\xi} \\ 0 & 0 & 0 & 0 \end{pmatrix}, \tag{A 7}$$

and

$$\boldsymbol{D}_1 = \begin{pmatrix} 0 & 2X_{01\xi} & 0 & Y_{01} \\ (Y_{01} - 2X_{01\xi}) & 0 & (Y_{01} - 3X_{01\xi}) & Y_{01\xi} \\ 0 & -2X_{01\xi} & 0 & -Y_{01} \\ 0 & 0 & 0 & 0 \end{pmatrix}, \tag{A 8}$$

and

$$\boldsymbol{E}_1 = \begin{pmatrix} 0 & 0 & 0 & 0 \\ 0 & 0 & 0 & 0 \\ 0 & X_{01\xi} & 0 & 0 \\ 0 & Y_{01\xi} & 0 & 0 \end{pmatrix}. \tag{A 9}$$

REFERENCES

Akers, B. & Nicholls, D. P. 2012 Spectral stability of deep two-dimensional gravity water waves: repeated eigenvalues. *SIAM J. Appl. Math.* **72** (2), 689–711.

Benjamin, T. B. 1967 Instability of periodic wavetrains in nonlinear dispersive systems. *Proc. Roy. Soc. Lond. A.* **299** (1456), 59–76.

Benjamin, T. B & Feir, J. E. 1967 The disintegration of wave trains on deep water part 1. theory. *J. Fluid Mech.* **27** (03), 417–430.

Blyth, M. G. & Părău, E. I. 2016 The stability of capillary waves on fluid sheets. *J. Fluid Mech.* **806**, 5–34.

Chen, B. & Saffman, P. G. 1985 Three-dimensional stability and bifurcation of capillary and gravity waves on deep water. *Stud. Appl. Math.* **77** (2), 125–147.

Choi, W. 2009 Nonlinear surface waves interacting with a linear shear current. *Math. and Comput. Simul.* **80** (1), 29–36.

Crapper, G. D. 1957 An exact solution for progressive capillary waves of arbitrary amplitude. *J. Fluid Mech.* **2** (06), 532–540.

Deconinck, B. & Oliveras, K. 2011 The instability of periodic surface gravity waves. *J. Fluid Mech.* **675**, 141–167.

Deconinck, B. & Trichtchenko, O. 2014 Stability of periodic gravity waves in the presence of surface tension. *Eur. J. Mech.-B/Fluids* **46**, 97–108.

Dyachenko, A. I., Zakharov, V. E. & Kuznetsov, E. A. 1996 Nonlinear dynamics of the free surface of an ideal fluid. *Plasma Phys. Rep.* **22**, 829–840.

Dyachenko, S. A. & Hur, V. M. 2019*a* Stokes waves with constant vorticity: folds, gaps and fluid bubbles. *J. Fluid Mech.* **878**, 502–521.

Dyachenko, S. A. & Hur, V. M. 2019*b* Stokes waves with constant vorticity: I. numerical computation. *Studies Appl. Math.* **142** (2), 162–189.

Hogan, S. J. 1988 The superharmonic normal mode instabilities of nonlinear deep-water capillary waves. *J. Fluid Mech.* **190**, 165–177.

Hur, V. M. & Vanden-Broeck, J.-M. 2020 A new application of crapper's exact solution to waves in constant vorticity flows. *Euro. J. Mech-B/Fluids* **83**, 190–194.

Hur, V. M. & Wheeler, M. H. 2020 Exact free surfaces in constant vorticity flows. *J. Fluid Mech.* **896**.

Kapitula, T. & Promislow, K. 2013 *Spectral and dynamical stability of nonlinear waves*. Springer.

Lighthill, M. J. 1965 Contributions to the theory of waves in non-linear dispersive systems. *IMA J. Appl. Math.* **1** (3), 269–306.

Longuet-Higgins, M. S. 1978 The instabilities of gravity waves of finite amplitude in deep water i. superharmonics. *Proc. Royal Soc. Lond.. A.* **360** (1703), 471–488.

McLean, J. W. 1982 Instabilities of finite-amplitude water waves. *J. Fluid Mech.* **114**, 315–330.

Murashige, S. & Choi, W. 2020 Stability analysis of deep-water waves on a linear shear current using unsteady conformal mapping. *J. Fluid Mech.* **885**.

Saffman, P. G. 1985 The superharmonic instability of finite-amplitude water waves. *J. Fluid Mech.* **159**, 169–174.

Tanaka, M. 1983 The stability of steep gravity waves. *J. Phys. Soc. Japan* **52** (9), 3047–3055.

Tiron, R. & Choi, W. 2012 Linear stability of finite-amplitude capillary waves on water of infinite depth. *J. Fluid Mech.* **696**, 402–422.

Vanden-Broeck, J.-M. 1996 Periodic waves with constant vorticity in water of infinite depth. *IMA J. Appl. Math.* **56** (3), 207–217.

Whitham, G. B. 1967 Non-linear dispersion of water waves. *J. Fluid Mech.* **27** (2), 399–412.